Results in Engineering 31 (2026) 111479

Contents lists available at ScienceDirect

Results in Engineering

journal homepage: www.sciencedirect.com/journal/results-in-engineering

Research paper

Techno-Economic integration of OTEC thermodynamic cycles with the development of floating prototype model in North Bali

Ahmad M. Firdaus [a,*], Adriani Phady [b], Ristiyanto Adiputra [c]

[a] Coastal Engineering Research Group, Ocean Engineering Program, Faculty of Civil Engineering- New and Renewable Energy Research Centre, Institut Teknologi Bandung (ITB), Indonesia
[b] Ocean Engineering Master Program, Faculty of Civil Engineering, Institut Teknologi Bandung (ITB), Indonesia
[c] Research Center for Hydrodynamics Technology, National Research and Innovation Agency (BRIN), Tangerang Selatan, 15310, Indonesia

ARTICLE INFO

Keywords:
Ocean thermal energy conversion
Rankine cycle
Aspen plus V14
Levelized cost of energy
Floating barge

ABSTRACT

Ocean Thermal Energy Conversion (OTEC) provides a continuous, low-carbon electricity source for tropical regions with stable ocean temperature gradients. Floating OTEC systems are particularly attractive for archipelagic countries, as they enable access to deep cold seawater while avoiding coastal land constraints. This study presents an integrated techno-economic assessment of a floating closed-cycle OTEC plant proposed for North Bali, Indonesia. Three thermodynamic configurations—the Rankine, Kalina, and Uehara cycles—are evaluated using Aspen Plus simulations and validated against published numerical and experimental studies. Site-specific seawater temperatures of 29.28 °C (surface) and 5.29 °C (deep water) are applied. The results show that the Uehara cycle achieves the highest thermal efficiency at 3.3%, followed by the Kalina cycle at 3.0%, and the Rankine cycle at 2.1%. In net power output, the Uehara cycle leads with 11.724 MW, followed by the Rankine cycle at 11.086 MW and the Kalina cycle at 10.081 MW. However, considering simplicity, operational reliability, and offshore suitability, the single Rankine cycle is chosen for the floating OTEC prototype. Despite slightly lower performance, its simpler design and easier control make it the most practical option for initial deployment under the site conditions. Preliminary buoyancy and stability analyses confirm adequate reserve buoyancy and compliance with offshore stability criteria. Economic evaluation over a 30-year lifetime yields a levelised cost of electricity of Rp 2164–2313/kWh and an equity payback period of approximately four years, indicating strong potential for floating OTEC deployment in tropical island regions.

1. Introduction

The transition toward low-carbon energy systems has become increasingly urgent due to rising global energy demand, climate change, and the environmental impacts of fossil-fuel dependence. Indonesia remains heavily dependent on fossil fuels, with coal, oil, and natural gas accounting for approximately 44%, 23%, and 21% of total energy production, respectively [1]. This dependence contributes significantly to greenhouse-gas emissions and climate-related risks. With the population projected to reach about 285 million by 2025 [2] and electricity demand expected to grow to 1491 TWh by 2040 [1], ensuring reliable and sustainable electricity supply-particularly for remote and island regions-remains a major national challenge.

Ocean Thermal Energy Conversion (OTEC) is a marine renewable energy technology that utilizes the temperature difference between warm surface seawater and cold deep seawater to generate electricity. Practical operation typically requires a temperature difference exceeding 20 °C [3,4], which is consistently available in tropical regions. Theoretical global OTEC potential has been estimated at up to 30 TW [4], indicating its long-term relevance as a baseload renewable energy source. For archipelagic countries such as Indonesia, OTEC provides an opportunity to utilize indigenous marine resources while supporting national energy security and sustainability targets aligned with SDG 7 and SDG 13 [1,5]. This persistent fossil-fuel dependence highlights the urgency of transition strategies, including carbon mitigation and clean energy diversification schemes. In addition to alternative chemical energy loops—such as water-gas shift reactions optimized via carbon dioxide capture—the utilization of indigenous, continuous marine energy sources presents an exceptional path toward stabilizing tropical island grids [6].

* Corresponding author.
E-mail address: ahmad.firdaus@itb.ac.id (A.M. Firdaus).

https://doi.org/10.1016/j.rineng.2026.111479
Received 9 January 2026; Received in revised form 24 May 2026; Accepted 8 June 2026
Available online 9 June 2026

Bali Province has established renewable-energy targets through the Regional Energy General Plan (RUED) 2020–2050. Despite favorable oceanographic conditions in [1]northern Bali, renewable deployment remains dominated by land-based technologies, while marine energy systems such as OTEC are largely unexplored [7]. Previous studies have indicated promising OTEC potential in Indonesian waters. Ilahude et al. [8] reported temperature differences of 22–25 °C in North Bali with an estimated potential of 71.1 MW, while Yudananta [9] estimated that a land-based closed-cycle OTEC system could generate approximately 10 MW.

Recent research has explored improvements in OTEC thermodynamic cycles, heat-exchanger technologies, and offshore system integration [10–12]. Closed-cycle systems are commonly preferred for offshore deployment due to their relatively simple configuration and operational stability [11]. Among them, the Rankine, Kalina, and Uehara cycles have been proposed to enhance performance under the small temperature gradients typical of OTEC systems. However, most studies focus primarily on thermodynamic performance, while integrated assessments that simultaneously consider cycle selection, floating-platform integration, and economic feasibility remain limited, particularly for site-specific applications in Indonesia.

This study addresses this gap by conducting an integrated techno-economic assessment of a floating closed-cycle OTEC system in North Bali. The primary objective is to identify the most suitable thermodynamic cycle for a floating OTEC prototype under local oceanographic conditions. To achieve this, three closed-cycle configurations-Rankine, Kalina, and Uehara-are evaluated using Aspen Plus simulations. The study further aims to: (1) compare the thermodynamic performance of the three cycles, (2) integrate the selected cycle with a conceptual floating OTEC platform, and (3) evaluate the system's techno-economic feasibility through analysis of capital expenditure (CAPEX), operating expenditure (OPEX), and levelized cost of electricity (LCOE).

2. Closed-Cycle OTEC technology

2.1. General thermodynamic framework

Closed-cycle OTEC systems generate electricity by circulating a low-boiling-point working fluid between a warm seawater heat source and a cold seawater heat sink. Compared with open and hybrid systems, closed-cycle configurations offer continuous operation, simpler control requirements, and lower technical risk [13]. These characteristics make them particularly suitable for floating applications.

In all closed-cycle configurations, power generation proceeds through four fundamental thermodynamic processes: evaporation, expansion, condensation, and pumping. The working fluid—typically ammonia or an ammonia–water mixture—undergoes repeated phase change, enabling continuous conversion of low-grade thermal energy into mechanical work and subsequently electrical power [14]. Given the small temperature differences available in OTEC systems, cycle performance is highly sensitive to heat-transfer effectiveness, irreversibility, and auxiliary power consumption.

2.2. Main system components

The evaporator acts as a heat exchanger in which pressurised liquid working fluid absorbs heat from warm surface seawater, typically at temperatures of 26–30 °C, and vaporises. The low boiling temperature of the working fluid enables evaporation under these modest thermal conditions. Evaporator effectiveness has a direct influence on turbine inlet conditions and overall cycle efficiency.

The vapour generated in the evaporator expands through the turbine, producing mechanical power that is converted to electricity via a generator. Expansion is generally quasi-isentropic, resulting in a reduction in pressure and temperature at the turbine outlet. Following expansion, the low-pressure vapour enters the condenser, where it rejects heat to cold deep seawater, typically at temperatures of 4–8 °C, and condenses to a liquid state. Complete condensation is required to ensure stable pump operation and to minimise cavitation risks.

Finally, the condensed working fluid is pressurised by a pump and returned to the evaporator. Although pumping consumes mechanical power, its contribution to the total energy balance is small compared with turbine output, but it remains important in net power and economic assessments.

2.3. Closed-Cycle configurations

- *Rankine Cycle*

The Rankine Cycle is the simplest closed-cycle configuration for OTEC applications and employs a single-component working fluid, most commonly ammonia. Owing to its simplicity and robustness, it is frequently used as a benchmark in techno-economic studies. Typical operating conditions include evaporator pressures of 1–2 MPa and warm seawater temperatures of 26–30 °C. The specific turbine work is expressed as:

$$\boldsymbol{w}_{tur,Rankine} = \boldsymbol{h}_6 - \boldsymbol{h}_{10}$$

The power consumption of the working-fluid pump is given by [4]:

$$W_{refr} = \frac{m_{refr}(h_3 - h_2)}{\eta_{refr}}$$

Although the Rankine Cycle can achieve relatively high thermal efficiency, its net power output is limited by the absence of internal heat recovery. The integration of ejectors has been shown to improve net power output by approximately 12–15% by increasing turbine inlet pressure and reducing outlet pressure [11].

- *Kalina Cycle*

The Kalina Cycle employs an ammonia–water mixture as the working fluid, enabling improved thermal matching with low-temperature heat sources. By varying the ammonia concentration, phase change occurs over a temperature range rather than at a constant temperature, thereby reducing thermodynamic irreversibilities relative to the Rankine Cycle.

To enable internal heat recovery and composition control, the Kalina Cycle incorporates additional components such as separators, recuperators, diffusers, and mixers [13]. While these features can improve gross thermal efficiency, the increased system complexity and auxiliary power consumption can significantly reduce net power output under OTEC operating conditions.

- *Uehara Cycle*

The Uehara Cycle is an advanced modification of the Kalina Cycle, developed to maximise energy extraction from very small temperature gradients. It consists of two interacting ammonia–water loops and incorporates staged expansion, regenerators, heaters, and multiple pumps to intensify internal heat recovery.

Thermal efficiencies of up to 5.4% have been reported, approximately 10% higher than those of the Kalina Cycle [11]. However, these gains are achieved at the expense of increased system complexity, with implications for capital cost, control requirements, and operational reliability in floating applications.

3. Thermodynamic simulation

3.1. Model validation

Model validation is an important initial step to ensure that the developed simulation model and method can reproduce the

performance reported in previous studies. In this research, each thermodynamic cycle was validated using different reference studies that represent similar system configurations.

The Rankine cycle was validated based on the study conducted by Bharathan et al. [15], which reported a net power output of 13 MW under warm and cold seawater temperatures of 26 °C and 4.5 °C, respectively. For the Kalina cycle, validation refers to the study conducted by Ogriseck [14], which investigated the Kalina cycle for geothermal applications. This reference was selected because studies providing detailed validation of the Kalina cycle specifically for OTEC applications are still limited. In the reference study, the system used a warm geothermal fluid temperature of 120 °C and a cold water temperature of 5 °C, with an ammonia–water mixture as the working fluid and an ammonia mass fraction of 82 percent. The reported net power output was approximately 2.2 MW. After the model was validated under these reference conditions, the input parameters were adjusted to represent the operating conditions of the OTEC system, which has a significantly lower warm water temperature compared to geothermal systems.

For the Uehara cycle, the validation was based on experimental results reported by Goto et al. [17]. The validation process began by inputting the main parameters from the reference study and then supplementing them with analytical calculation results that describe the thermodynamic conditions at each state point of the cycle. The validation was carried out by comparing the simulated net power output with the reported target power output of approximately 30 kW. The main input parameters used for validating each cycle are summarized in Table 1.

The thermodynamic validation process was conducted using Aspen Plus V14, which is capable of simulating thermodynamic components within a complete cycle. The simulation method for all cycles applied the Peng–Robinson equation of state, which is widely used to represent working fluid properties and heat transfer processes within thermodynamic systems.

The validation results of each cycle obtained from the Aspen Plus simulations are presented in Fig. 1. The thermodynamic properties at each state point are summarized in Table 2, while the comparison of the error values for the main output parameters is presented in Table 3. The simulation results show that the thermodynamic conditions at each state point are consistent with those reported in the reference studies. In addition, the deviation in the calculated power output for each cycle remains relatively small. Therefore, the developed simulation models are considered sufficiently accurate and can be used for further analysis in this study.

The model validation in this study employed operating conditions from previous studies to verify the thermodynamic cycle configuration, system behavior, simulation consistency, and mathematical convergence of the Peng–Robinson equation of state for multi-component mixtures. Although the reference operating conditions used for validation, particularly the 124 °C geothermal heat source temperature in the Kalina cycle, differ significantly from the marine thermal gradient under the site-specific OTEC conditions, the validation remains sufficient to confirm the robustness and predictive capability of the developed thermodynamic model. The thermodynamic formulations and phase-equilibrium property methods applied in the simulation remain valid under lower temperature gradients. Application of the model to the North Bali oceanographic profile of 29.28 °C and 5.29 °C primarily affects the magnitude of enthalpy change and the achievable gross power output without altering the fundamental thermodynamic consistency of the model. Therefore, the validated thermodynamic framework can be reliably applied to simulate site-specific OTEC conditions using local environmental parameters. The simulation results further provide an estimation of the minimum operational conditions and component performance required to achieve the targeted net power output.

Table 1
Validation Simulation Parameters.

Parameters	Unit	Rankine Cycle	Kalina Cycle	Uehara Cycle
Warm Seawater Temperature	°C	26	124	29
Cold Seawater Temperature	°C	4,5	5	8,02
Mass Flowrate Warm Seawater	kg/s	50.000	89	194,17
Mass Flowrate Cold Seawater	kg/s	28.450	-	110,56
Ammonia Mass Flowrate	kg/s	585	16.8	2,06
Pumps Efficiency	%	72	98	95
Turbine Efficiency	%	75	87	65
Working Fluid material	-	Ammonia	Ammonia - water	Ammonia - Water
Ammonia fraction	%	100	82	95
Gross Power Output	kW	18,381	2194.8	26.53
Net Power Output	kW	13,608	-	-

3.2. Performance at site-specific conditions

The performance analysis of each thermodynamic cycle was evaluated under site-specific conditions in the North Bali Sea. Based on local oceanographic measurement data, the site exhibits a warm surface seawater temperature of 29.28 °C and a deep cold seawater temperature of 5.29 °C at a target depth of 700 m. These baseline values were utilized to assess and compare the operational efficiency of the proposed configurations. To ensure a standardized comparative framework, all operational parameters other than temperature were kept constant across all cycles. The complete matrix of site-specific input parameters is summarized in Table 4.

Under the site-specific simulation conditions, the target net power output was set at 10 MW. For the single Rankine cycle and Kalina cycle, the turbine rated power was set at 15 MW, while the Uehara cycle used two turbines with a rated power of 7.5 MW each. The temperature difference between the inlet and outlet seawater (ΔT) used in the initial analysis was 3 °C, while the seawater mass flow rate was adjusted according to the system requirements to achieve the desired power output. For the Kalina and Uehara cycles, the working fluid used was an ammonia–water mixture with an ammonia mass fraction of 82%. The simulation results obtained using these site-specific parameters are presented in Fig. 2, while the comparison of the power output generated by each cycle is shown in Table 5.

3.3. Sensitifity analysis

Sensitivity analysis was conducted on several key parameters, namely the temperature difference between inlet and outlet seawater (ΔT) and the efficiency of the seawater pump. This analysis aims to evaluate the influence of changes in input parameters on the performance of the cycle system being studied. In the initial analysis, the ΔT value was set at 3 °C, and further analysis was carried out using variations of 2 °C and 4 °C. Other parameters were assumed to remain constant, while the seawater mass flow rate was adjusted to achieve the targeted temperature difference. In addition, the seawater pump efficiency, which was initially set at 80%, was further analyzed with efficiency variations of 75% and 85%.

The results of the analysis on the temperature difference parameter (ΔT) indicate that ΔT affects the thermal efficiency of the cycle. As the value of ΔT increases, the thermal efficiency also increases. This trend occurs in all cycles analyzed, where the Rankine cycle shows the lowest thermal efficiency, followed by the Kalina cycle, while the Uehara cycle exhibits the highest thermal efficiency. For example, in the Rankine cycle, the thermal efficiency increases from 1.74% at $\Delta T = 2$ °C to 2.1% at $\Delta T = 3$ °C, and further increases to 2.3% at $\Delta T = 4$ °C (see Fig. 3).

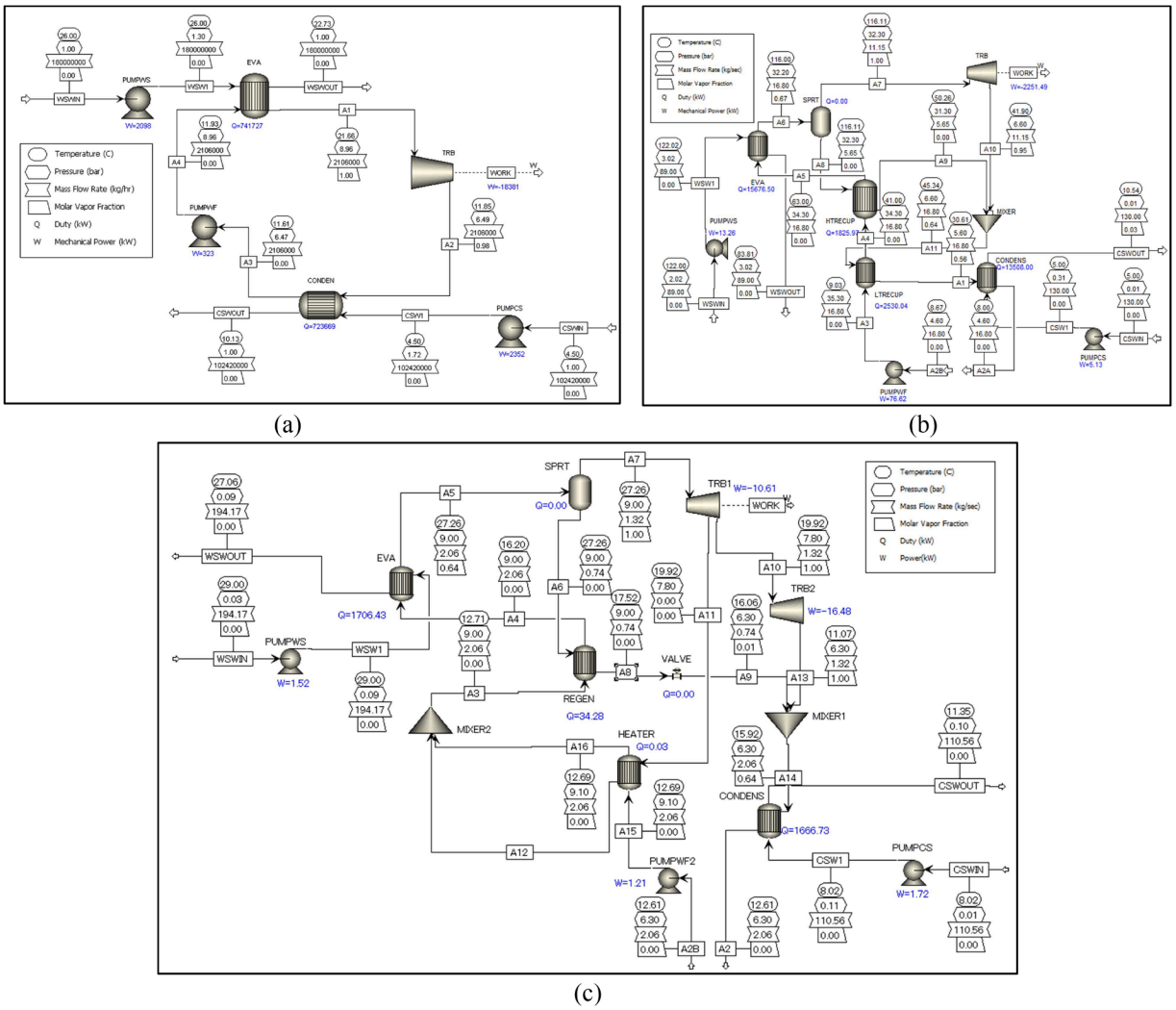

Fig. 1. Flowsheet Thermodynamic simulation Validation (a) Rankine Cycle (b) Kalina Cycle (c) Uehara Cycle.

The increase in thermal efficiency is influenced by changes in the seawater mass flow rate required to achieve the targeted ΔT value. Fig. 4 (a) shows the relationship between ΔT and the required seawater mass flow rate. The analysis results indicate that a smaller ΔT requires a larger mass flow rate. For example, in the Kalina cycle, when ΔT is 4 °C, the required warm seawater mass flow rate is about 19,000 kg/s. This value increases to around 25,000 kg/s at ΔT of 3 °C and further increases to approximately 36,000 kg/s when ΔT decreases to 2 °C.

The increase in mass flow rate directly affects the pumping power requirement. The larger the mass flow rate needed, the greater the pumping power required to circulate seawater within the system. This total pumping power requirement is commonly referred to as parasitic power, which is the power consumed to operate the cycle system and is deducted from the generated net power. The relationship between mass flow rate and parasitic power is illustrated in Fig. 4(b), showing that an increase in mass flow rate tends to increase parasitic power. In addition, the analysis results indicate that the Rankine cycle requires the highest mass flow rate among the analyzed cycles, which is followed by a relatively high parasitic power, reaching about 5860 kW at a mass flow rate of approximately 56,000 kg/s.

A clearer trend regarding the effect of ΔT on parasitic power can be observed in Fig. 5(a). The analysis results show that the Rankine cycle requires the highest parasitic power, followed by the Uehara cycle and the Kalina cycle. For the Kalina and Uehara cycles, the pumping power requirements are relatively similar, at approximately 3900 kW at ΔT of 2 °C, about 2700 kW at ΔT of 3 °C, and around 2100 kW at ΔT of 4 °C.

The magnitude of parasitic power directly affects the net power output of each cycle. Fig. 5(b) illustrates the influence of ΔT on net power output. Although the gross power produced is relatively similar for each ΔT target, the higher parasitic power at smaller ΔT values results in lower net power output. Conversely, when ΔT increases, the required parasitic power decreases, which leads to an increase in net power output.

The analysis results indicate that the Uehara cycle produces the highest net power output at ΔT of 4 °C, reaching approximately 12,500 kW, followed by the Rankine cycle and the Kalina cycle. Meanwhile, the Kalina cycle generates the lowest net power output because the gross power produced under these input parameters is relatively smaller compared to the other cycles, resulting in a lower net power output.

The results of the sensitivity analysis on pump efficiency can be seen in Fig. 6. With other parameters kept constant and ΔT set at 3 °C, the analysis shows that higher pump efficiency results in lower parasitic power requirements. This trend occurs in all analyzed cycles, where the Rankine cycle produces the highest parasitic power, followed by the Uehara cycle and the Kalina cycle.For example, in the Uehara cycle, when the pump efficiency is 75%, the required parasitic power is about 2937 kW. This value decreases to around 2768 kW when the pump efficiency increases to 80%, and further decreases to approximately 2600 kW when the pump efficiency reaches 85%. This trend indicates that increasing pump efficiency can reduce the power required to operate the

Table 2
Parameter of key state point each cycle.

Cycle	State Point	Temperature (°C)		Fraction		Pressure (bar)		Mass flowrate (kg/s)	
		Ref.	Result	Ref.	Result	Ref.	Result	Ref.	Result
Rankine Cycle	1	21.38	21.66	-	1	8.96	8.96	580	580
	2	11.61	11.85	-	0.98	6.47	6.49	580	580
	3	11.61	11.85	-	0	6.47	6.47	580	580
	4	11.72	11.93	-	0	8.96	8.96	580	580
Kalina Cycle	1	30	30.61	0.56	0.56	5.6	5.6	16.8	16.8
	2	8	8	0	0	4.6	4.6	16.8	16.8
	3	8	8.35	0	0	35.3	35.3	16.8	16.8
	4	41	41	0	0	34.3	34.3	16.8	16.8
	5	63	63	0	0	33.3	33.3	16.8	16.8
	6	116	116	0.68	0.67	32.3	32.3	16.8	16.8
	7	116	116.11	1	1	32.3	32.3	11.4	11.15
	8	116	116.11	0	0	32.3	32.3	5.4	5.65
	9	46	50.26	0	0	31.3	31.3	5.4	5.65
	10	42	41.9	0.94	0.95	6.6	6.6	11.4	11.15
	11	46	45.34	0.64	0.64	6.6	6.6	16.8	16.8
Uehara Cycle	1	15.75	15.92	-	0.64	6.3	6.3	2.055	2.06
	2	12.32	12.61	-	0	6.3	6.3	2.055	2.06
	3	12.38	12.69	-	0	9	9.1	2.055	2.06
	4	15.77	16.2	-	0	9	9	2.060	2.06
	5	27.26	27.26	-	0.64	9	9	2.060	2.06
	6	27.26	27.26	-	1	9	9	1.443	1.317
	7	27.26	27.26	-	0	9	9	0.617	0.743
	10	11.07	11.07	-	1	6.3	6.3	1.438	1.317
	11	18.40	19.92	-	0	7.8	7.8	0.005	0.0023
	13	12.38	12.69	-	0	9	9.1	2.055	2.055
	15	18.40	18.17	-	0	7.8	7.8	0.005	0.0023

Table 3
Validation results on power output for each cycle.

Parameters	Rankine Cycle			Kalina Cycle			Uehara Cycle		
	Ref.	Result	Error	Ref.	Result	Error	Ref.	Result	Error
Gross Power Output (kW)	18,389	18,381	0.04%	2194.8	2251.4	2.5%	26.52	27.09	2.1%
Net Power Output (kW)	13,608	13,045	4.31%	-	-	-	-	-	-
Efficiency (%)	1.83	1.75	4.57%	-	-	-	-	-	-

Table 4
Parameters Input on Site-Specific Conditions.

Parameters	Units	Single Rankine	Kalina Cycle	Uehara Cycle
Power rated turbine (each turbine)	kW	15,000	15,000	7500
Hot sea water temperature	°C	29.28	29.28	29.28
Cold sea water temperature	°C	5.29	5.29	5.29
Turbine efficiency	%	85	85	85
Working fluid pump efficiency	%	75	75	75
Sea water pump efficiency	%	80	80	80
Seawater Temperature Difference	°C	3	3	3
Area evaporator	m^2	22,000	22,000	22,000
Area condenser	m^2	22,000	22,000	22,000
Overall Heat Transfer Coefficient	kW/m^2	5.56	5.56	5.56
Mass flow rate working fluid	kg/s	500	500	500
Working fluid		Ammonia	Ammonia-water mixture	Ammonia-water mixture
Fraction ammonia mixture	%	-	82	82

pumping system within the cycle.

Consistent with this trend, higher pump efficiency also has a positive impact on the net power output of each cycle. The reduction in parasitic power leads to an increase in the net power generated, although the improvement in net power output is relatively small. This relationship can be observed more clearly in Fig. 7.

4. Floating OTEC plant prototype design

Based on the performance analysis of the three OTEC configurations, namely the Rankine Cycle, Kalina Cycle, and Uehara Cycle, the thermodynamic performance of each cycle was evaluated under site-specific conditions in the North Bali Sea, where the measured seawater temperatures are 29.28 °C for warm surface seawater and 5.29 °C for deep seawater at a depth of approximately 700 m. Using identical design parameters for the main system components, the simulation results indicate that the Uehara cycle achieves the highest thermal efficiency of 3.3%, followed by the Kalina cycle with 3.0%, while the Rankine cycle exhibits a thermal efficiency of 2.1%.

In terms of power generation performance, the Uehara cycle produces the highest net power output of approximately 11.724 MW, followed by the Rankine cycle with 11.086 MW, and the Kalina cycle with 10.081 MW. The higher efficiency observed in the Kalina and Uehara cycles is mainly attributed to the use of an ammonia–water mixture working fluid, which improves the thermodynamic matching between the heat source and the working fluid during the evaporation process. However, these cycles also involve more complex system configurations and operational control due to the presence of multi-component working fluids and additional separation processes.

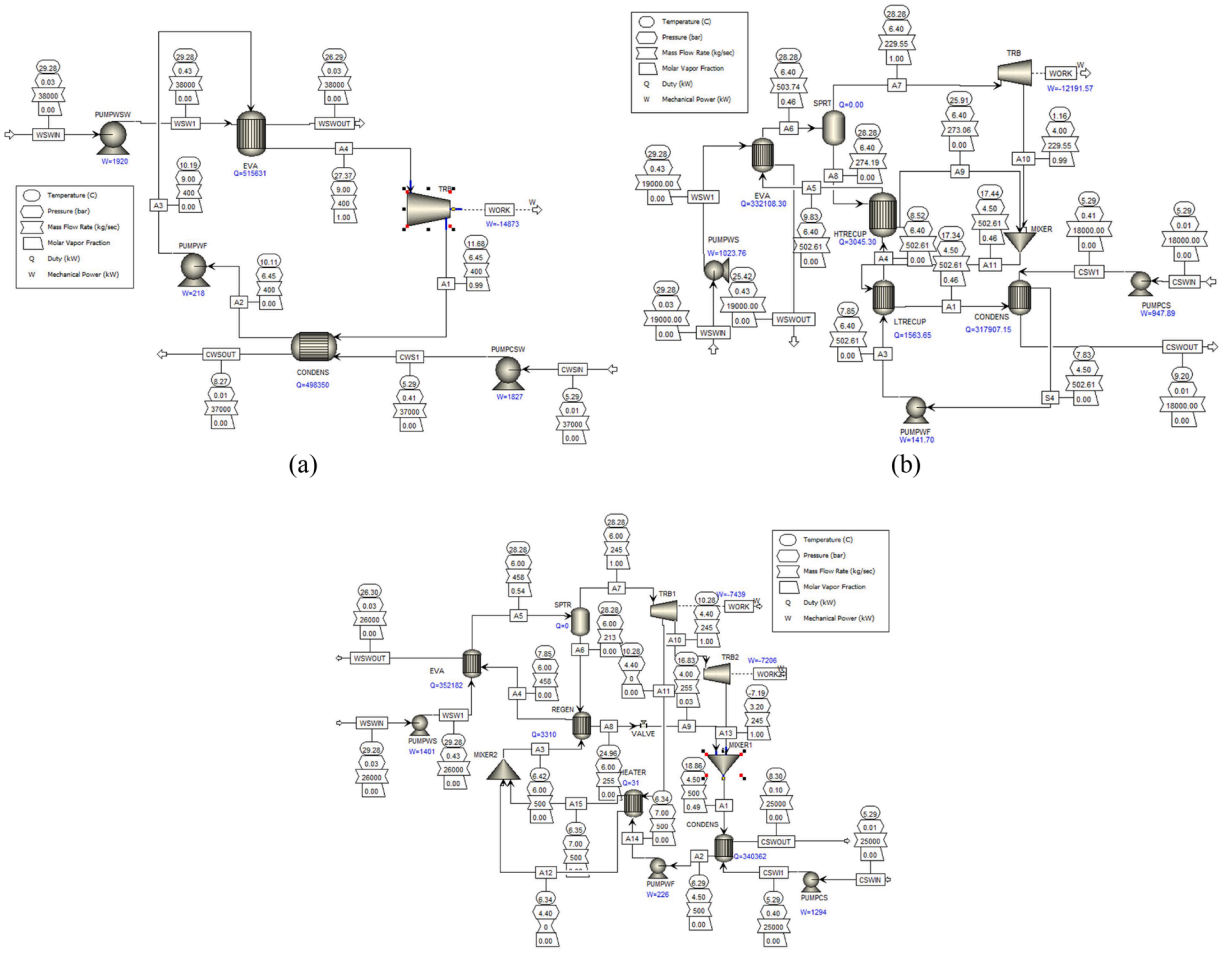

Fig. 2. Flowsheet Thermodynamic simulation on specific site (a) Rankine Cycle (b) Kalina Cycle (c) Uehara Cycle.

Table 5
Results on Site-Specific.

Parameters	Units	Rankine Cycle	Kalina Cycle	Uehara Cycle
Gross Power	kW	15,000	12,192	14,645
Working Fluid Pump Power	kW	218	184	242
Warm Seawater Pump Power	kW	1920	1262	1313
Cold Seawater Pump Power	kW	1827	1184	1213
Net Power	kW	11,086	10,081	11,724
Efficiency	%	2.1	3	3.3

Considering the balance between system simplicity, operational stability, and practical implementation for a floating offshore system, the single Rankine Cycle is selected as the basis for the floating OTEC prototype design in this study. Although the Uehara cycle shows slightly higher thermodynamic performance, the Rankine cycle offers a simpler configuration with fewer components and easier operational control, making it more suitable for the development of an initial floating OTEC prototype under the site conditions considered in this research.

4.1. Main system components

The primary components of the OTEC system include the riser system, heat exchangers, turbine-generator units, and pumps. The risers function as the main conduits for transporting deep cold seawater and warm surface seawater to the system and discharging the seawater back to the ocean after heat exchange. The heat exchangers transfer thermal energy from warm seawater to the working fluid to induce evaporation and subsequently condense the working fluid using cold seawater.

The turbine-generator converts the thermal energy of the pressurized working fluid into mechanical energy and subsequently into electrical power. Pumps are responsible for maintaining continuous circulation of seawater and working fluid at the required flow rates, ensuring stable and uninterrupted system operation. The integration of these components enables continuous electricity generation by exploiting the temperature difference between surface and deep seawater.

4.2. Riser design

The riser system is designed to transport seawater between the ocean and the onboard seawater tanks. Four risers are suspended beneath the plantship: cold water inlet (CWP inlet), cold water outlet (CWP outlet), warm water inlet (WWP inlet), and warm water outlet (WWP outlet).

Riser wall thickness is estimated using an empirical approach commonly applied in offshore oil and gas riser design. The characteristics of the cold water pipe are adopted from the study by Adiputra et al. (2020). The cold water pipe (CWP) is constructed using a sandwich fiberglass-reinforced plastic (FRP) structure, with a laminate density of 4125 kg/m^3, syntactic foam density of 1015 kg/m^3, elastic modulus of 13,776 MPa, and flexural rigidity of 2.89 $\times$ 10^{11} Nm^2. The estimated riser dimensions are summarized in Table 6.

It must be noted that the current structural dimensions are derived from empirical formulations and represent a primary hydrostatic design.

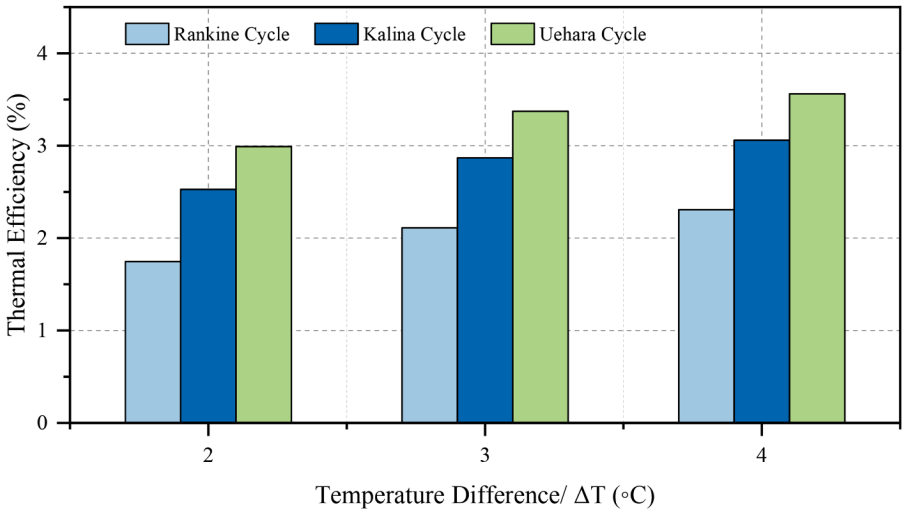

Fig. 3. Effect of seawater temperature difference on thermal efficiency.

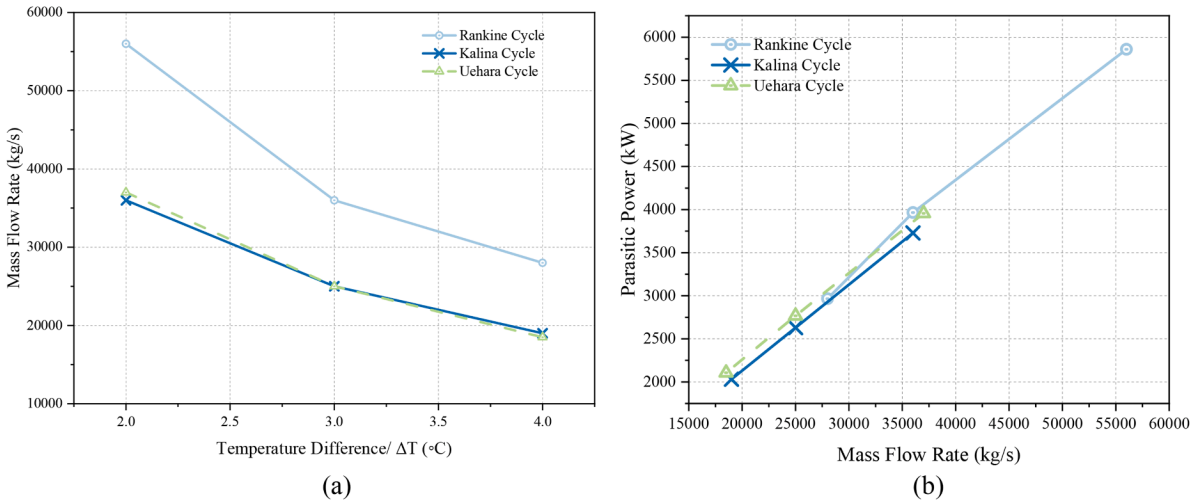

Fig. 4. Effect of Seawater Temperature Difference (a) on Mass Flow Rate Warm Seawater (b) Effect of Mass Flow Rate on Parasitic Power.

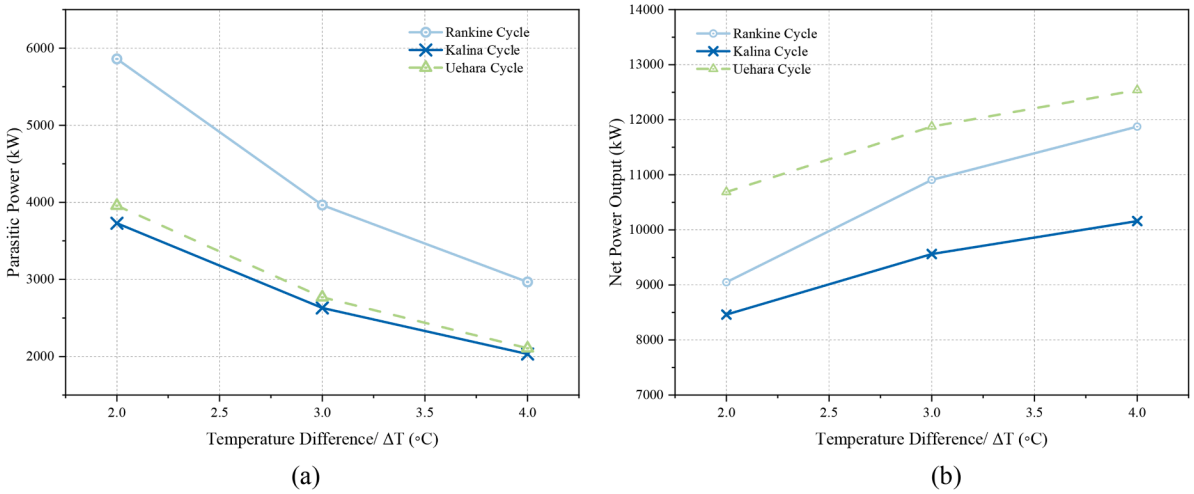

Fig. 5. Effect of seawater temperature difference on (a) Parasitic Power (b) Net Power Output.

In an operational offshore deployment, a 700-meter suspended cold water pipe is inherently subjected to critical hydro-elastic and dynamic loading. These include Vortex-Induced Vibrations (VIV) driven by deep ocean current profiles, complex wave-current interactions within the

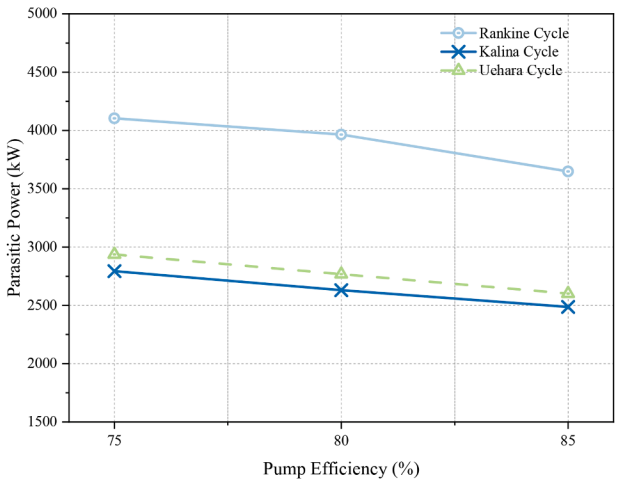

Fig. 6. Effect of Pump Efficiency on Parasitic Power.

wave zone, and cumulative fatigue stresses over the 30-year design life. Consequently, comprehensive hydrodynamic routing and finite-element dynamic analysis remain mandatory next steps to evaluate structural mitigation strategies, such as the deployment of helical strakes or aerodynamic fairings.

4.3. Heat exchangers, turbine–generator, and pumps

In this study, a simplified modular heat exchanger configuration is adopted. Based on thermal calculations, the required heat transfer area is approximately 22,000 m^2 for the evaporator and 22,000 m^2 for the condenser. These areas are distributed across 24 plate heat exchanger (PHE) units on each side, resulting in a total of 48 PHE units. Each unit provides approximately 900 m^2 of heat transfer area, with dimensions of 3.2 m × 2.6 m × 3.8 m.

The multi-unit configuration enhances operational reliability, promotes uniform flow distribution, and facilitates maintenance. Plate heat exchangers are selected due to their high heat transfer coefficients, compact size, and ease of cleaning through clean-in-place (CIP) systems to mitigate biofouling and scaling. Titanium or titanium alloy materials are employed to ensure corrosion resistance in seawater environments.

During operation, the evaporator vaporizes ammonia using warm seawater at an average temperature of 29.28 °C, while the condenser condenses ammonia vapor using cold seawater at 5.29 °C.

The turbine converts thermal energy into mechanical power as ammonia expands from 9 bar to 6.52 bar, yielding a gross power output of 15 MW. To ensure operational safety and redundancy, two parallel turbine units are installed, each rated at approximately 10 MW. This configuration improves reliability, load flexibility, and maintenance accessibility. With a turbine efficiency of 85%, the resulting net power output after accounting for pumping losses is 11 MW.

An axial-flow reaction turbine is selected due to its suitability for high mass flow rates and low pressure differences typical of OTEC systems. Each turbine–generator set has an estimated envelope dimension of 8 m × 4 m × 4.5 m, including auxiliary equipment. A synchronous generator with a secondary seawater-based cooling system is employed. The volumetric requirements of the main components are summarized in Table 7.

Pumping systems consist of warm seawater pumps (WWP), cold seawater pumps (CWP), and ammonia circulation pumps (AP). Warm seawater is supplied at 37,000 kg/s using 14 operating pumps and 3 standby units, while cold seawater at 36,000 kg/s is supplied by 8 operating pumps and 2 standby units. Ammonia circulation is maintained at 500 kg/s using 2 operating and 2 standby canned-motor pumps to prevent working-fluid leakage.

4.4. Buoyancy requirement

The buoyancy requirement analysis was conducted by compiling the weights of all main and auxiliary components of the floating OTEC barge

Table 6
Main dimensions of risers.

Riser	Length (m)	t FRP (cm)	T Foam (cm)	Volume Flow Rate (m^3/s)	Outside Diameter (m)
Cold Water Inlet (CWP inlet)	700	2.0	14.0	28.09	3,53
Cold Water Outlet (CWP outlet)	40	0,8	7.2	28.24	1.81
Warm Water Inlet (WWP inlet)	10	0.5	5.5	16,84	2.40
Warm Water Outlet (WWP outlet)	40	0.8	7.2	16.78	2.39

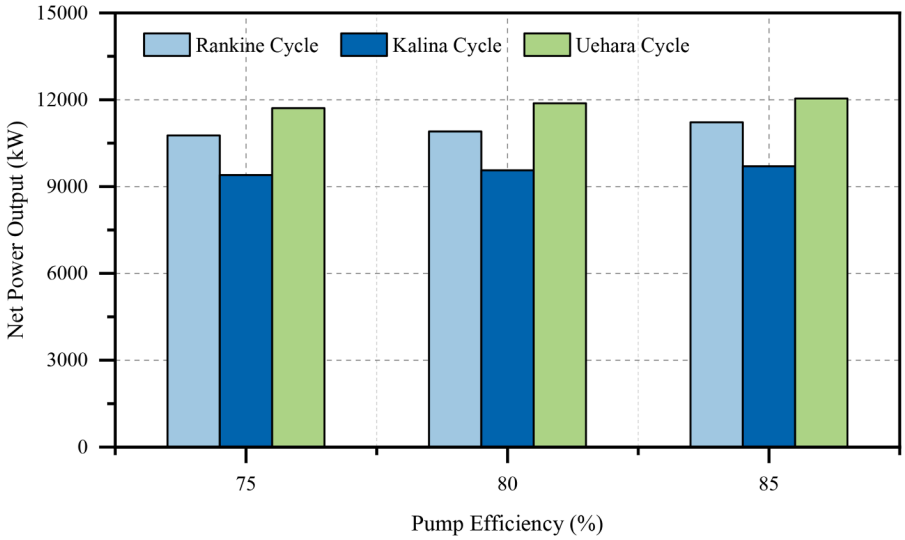

Fig. 7. Effect of Pump Efficiency on Net Power Output.

Table 7
Volumetric requirements of major components.

Items	Total	Units	Volumetric spaces
Turbine-Generator	2 *units*	*Core dimension*	8 m (L) × 4 m (W) × 4.5 m (H)
		Total dimension	20.5 m (L) × 6.5 m (W) × 6 m (H)
Evaporator and Condenser	24 *submodules each*	*Evaporator located above the seawater tank*	
		30 MW-*gross assembly*	3.2 m (L) × 2.6 m (W) × 3.8 m (H)
		Total dimension	30 m (L) × 12.6 m (W) × 4.8 m (H)
		Condenser located above the seawater tank	
		30 MW-*gross assembly*	3.2 m (L) × 2.6 m (W) × 3.8 m (H)
		Total dimension	30 m (L) × 12.6 m (W) × 4.8 m (H)
Pump	27 *units*	*Warm water pump* (17 *units*)	38 m (L) × 12.6 m (W) × 2.7 m (H)
		Cold water pump (10 *units*)	20 m (L) × 12.6 m (W) × 2.7 m (H)
		Ammonia pump (4 *units*)	10 m (L) × 12.6 m (W) × 3 m (H)

to determine the total system weight. The corresponding displacement was then calculated to estimate the operational draft, and the buoyancy margin was evaluated by comparing the maximum design displacement with the actual system weight. The weight breakdown of the barge is summarized in Table 8, which categorizes the loads into deadweight (DWT), lightweight (LWT), main components, and miscellaneous items. Based on this inventory, the total weight of the floating OTEC barge system is 5374 tons.

The displacement at the operational draft was calculated using the empirical formulation proposed by Rawson and Tupper [15].

$$\Delta = L_{pp} \times B \times T \times C_b$$

where $L_{pp} = 90\,\text{m}$, $B = 15\,\text{m}$, and $C_b = 0.9$. The submerged volume was obtained from the ratio between total system weight and seawater density ($\rho = 1.025\,\text{t}/\text{m}^3$) [15]:

$$V = \frac{W_{total}}{\rho} = \frac{5,374}{1.025} \approx 5,242\ m^3$$

Accordingly, the operational draft of the barge is calculated as:

$$T = \frac{5,242}{90 \times 15 \times 0.9} \approx 4.3\ m$$

Under the maximum design condition with a depth (H) of 9 m, the maximum displacement reaches 11,208 tons. The buoyancy margin is evaluated using the following expression [16]:

$$Margin = \frac{Displacement - W_{total}}{Displacement} \times 100\%$$

The results indicate that the floating OTEC barge possesses a buoyancy reserve of approximately 52%, confirming sufficient capacity to accommodate additional loads, operational variations, and environmental effects without compromising flotation. The actual operational draft of 4.3 m remains well below the design limit, ensuring safe operation.

Table 8
wt Breakdown of the Floating OTEC Barge System.

No	Item Category	Weight (Tons)
Deadweight (DWT)		
1	CC&E (*Crew Clothing & Effects*)	0.010
2	WC&E (*Weight of Crew & Effects*)	2.988
3	*Provisions and Stores*	0.005
Lightweight (LWT)		
4	*Hull Steel Structure*	1193
Main Component		
5	*Equipment*	2738
6	*Risers*	362
Miscellaneous		
7	*Fresh Water Tank*	40
8	*Ballast Tank*	322
9	*Sewage Tank*	21
10	*Crane*	152
11	*Mooring System*	438
12	*Safety Equipment*	25
13	*Electrical Components*	80
Total System Weight		**5374**

4.5. Center of gravity analysis

The center of gravity (CG) analysis was performed to assess the overall stability of the floating OTEC barge. This analysis accounts for weight contributions from the lightweight structure (LWT), main equipment, storage tanks, ballast, mooring system, crane, electrical systems, and seawater risers.

Based on the weight summary presented in Table 8, the total system weight amounts to 5754 tons. The largest contributors include seawater storage tanks (cold and warm water tanks) with a combined weight of approximately 1274 tons, followed by major components such as the turbine-generator (180 tons), evaporator (480 tons), and condenser (480 tons). The mooring system contributes significantly, with a total weight of 438 tons, effectively lowering the overall vertical center of gravity. The mooring system contributes significantly, with a total weight of 438 tons, effectively lowering the overall vertical center of gravity. This system is conceptually modeled as an 8-line symmetric catenary spread mooring configuration utilizing high-tensile steel studlink chains to fulfil station-keeping criteria under prevailing monsoonal wind, wave, and current forces in the North Bali Sea. The determination of extreme environmental design loads, safety factors against line breakage, and maximum allowable platform excursion limits to prevent riser damage are designated for the subsequent phase of detailed mooring line routing analysis.

The most influential component in terms of vertical stability is the cold water pipe (CWP) inlet, which has an approximate length of 700 m. The dry weight of the riser is about 969 tons, located at a vertical position of $Z_o = -350\,\text{m}$, producing a downward moment of −339,296 ton·m.

This substantial moment significantly enhances the vertical stability of the barge. The vertical center of gravity is calculated using the standard formulation [15]:

$$KG_{Tot} = \frac{\sum (W \times Zo)}{\sum \text{W}}$$

The calculated total KG (VCG) is 3.8 m when the riser-induced vertical moment is excluded, indicating that the system's center of mass lies above the baseline, primarily influenced by the lightweight structure. This relatively low KG contributes positively to initial stability; however, final stability assessment requires further evaluation of KM, BM, GM, and the righting-arm (GZ) curve.

For the lightweight structure, the vertical center of gravity was estimated using the empirical formulation proposed by Watson [17]:

$$KG_{str} = \left[58.3 - 0.517(0.824 - C_{bd}) \cdot \left(\frac{L}{H}\right)^2\right] \cdot Ds \cdot 0.01$$

Using $Ds = 11$ m and $C_{bd} = 0.918$, the structural KG is calculated to be approximately 7 m.

The longitudinal center of gravity (LCG) was determined relative to the longitudinal center of buoyancy (LCB). With an LCB value of 31.32%, the resulting LCG is located 0.147 m from midship, indicating a nearly symmetric longitudinal weight distribution and minimizing the potential for excessive trim during operation.

4.6. Hydrostatic stability analysis

Hydrostatic stability analysis was conducted to evaluate the ability of the floating OTEC barge to maintain equilibrium under small perturbations. Key parameters examined include the metacentric height (GM), center of buoyancy (KB), transverse metacentric radius (BM), and the righting-arm (GZ) curve. The variation of displacement, wetted surface area, waterplane area, and stability-related parameters with draft is illustrated by the hydrostatic curves, as shown in Fig. 8.

The analysis is based on hydrostatic data obtained from hull modeling using Maxsurf software and evaluated against the stability criteria specified by Biro Klasifikasi Indonesia (BKI). Positive GM values across all draft conditions confirm that the barge possesses adequate restoring capability against heeling.

At the operational draft of 4.3 m, the calculated displacement is approximately 5340 tons, closely matching the total system weight of 5374 tons. This agreement validates the consistency of the buoyancy and stability assessment.

GZ curve evaluations were performed for two configurations: with the cold water pipe (CWP) and without the CWP. In the configuration including the CWP, the maximum GZ reaches 3.26 m at a heel angle of 50°, exceeding the value obtained without the CWP (2.94 m). This result indicates that the suspended mass of the CWP effectively functions as a natural ballast, enhancing restoring moments at moderate to large heel angles.

The hydrostatic curves further indicate that as the draft increases from 4 m to 6 m, displacement increases nearly linearly, while initial stability parameters such as BM, KM, and GM exhibit a moderate decrease. This behavior is typical for flat-bottom barge hulls due to variations in waterplane moment of inertia. Nevertheless, all calculated GM values remain well above the minimum requirement of 0.15 m specified by BKI [18], confirming that the barge maintains adequate stability throughout its operational range.

While the floating barge complies with all intact hydrostatic safety criteria defined by Biro Klasifikasi Indonesia (BKI), the present stability evaluation is bounded by static equilibrium conditions (p. 15). A comprehensive safety validation requires the assessment of dynamic stability criteria under wave actions and operational loading conditions (p. 15). Platform seakeeping behaviors—specifically roll, pitch, and heave motions in rough seas—as well as the dynamic sloshing effects inside the warm and cold seawater storage tanks, present key operational risks that are recognized as limitations of the current study phase and will be addressed in future numerical sea-trial simulations

4.7. General arrangement

The conceptual general arrangement was developed to ensure the constructability and operational feasibility of a 13 MW floating OTEC platform. The power generation system is symmetrically divided into two compartments to maintain balanced load distribution on the hull.

Seawater tanks are positioned at the lowest elevation (1500 mm) and directly connected to the cold and warm water pipes. Heat exchangers are installed above the tanks at an elevation of 5300 mm to minimize suction losses and simplify fluid distribution. Ammonia water tanks and pumps are also placed at this level to enhance working-fluid circulation efficiency.

Seawater pumps (warm water pumps and cold water pumps) are located at an elevation of 6300 mm, considering pressure requirements and maintenance accessibility. The turbine–generator unit is installed on the main deck (9000 mm) to ensure protection from seawater exposure, improve operational safety, and facilitate maintenance.

The marine piping system is designed with due consideration of stability and environmental aspects. The cold water pipe is positioned near the barge's center of gravity to preserve longitudinal stability, while the warm water pipe is installed at a depth of approximately 10 m. The discharge pipe is routed below the keel with a length of about 40 m to prevent mixing with surface seawater. Flow velocities are limited to approximately 3 m/s to maintain hydrodynamic efficiency and minimize environmental impact.

The conceptual general arrangement is illustrated in Figs. 9–13, presenting side and plan views at various elevations to support system integration and layout verification.

5. Economic analysis

This study evaluates the economic feasibility of a 11 MW net closed-cycle OTEC system installed on a floating barge in the waters of Bungkulan Village, Buleleng Regency, Bali. The assessment focuses on key economic indicators, including capital expenditure (CAPEX), operational expenditure (OPEX), levelized cost of energy (LCOE), revenue potential, and payback period, within the context of Indonesia's current energy policy framework. The analysis adopts a 30-year project lifetime, an 8% discount rate, and a capacity factor of 0.90, reflecting the base-load operational characteristics of OTEC systems. Unlike intermittent renewable sources such as solar and wind, OTEC utilizes the relatively stable temperature difference between surface seawater and deep seawater in tropical regions, enabling continuous operation throughout the year. Previous techno-economic studies of closed-cycle OTEC systems report capacity factors ranging between 85% and 95%, accounting for scheduled maintenance and operational downtime [19]. Therefore, a value of 90% was selected as a realistic and moderately conservative assumption for long-term operation.

The total CAPEX of the proposed OTEC system is estimated at approximately Rp 1.95 trillion, dominated by heat exchangers, submarine cable installation, the floating barge structure, mooring system, and the cold water pipe. Among the capital components, the heat exchanger

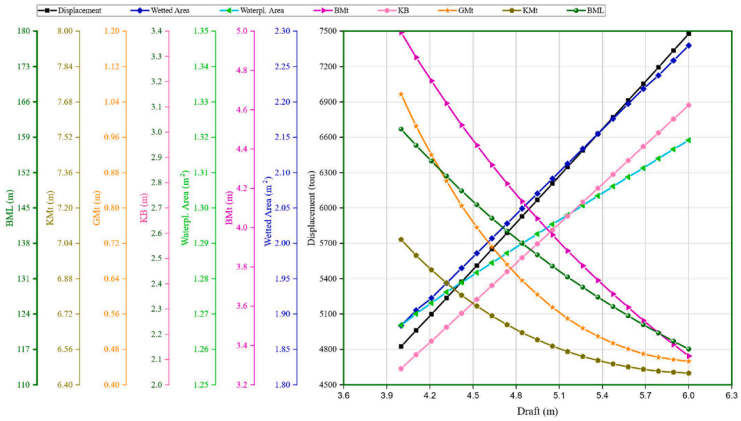

Fig. 8. Hydrostatic Curves of the Floating OTEC Barge.

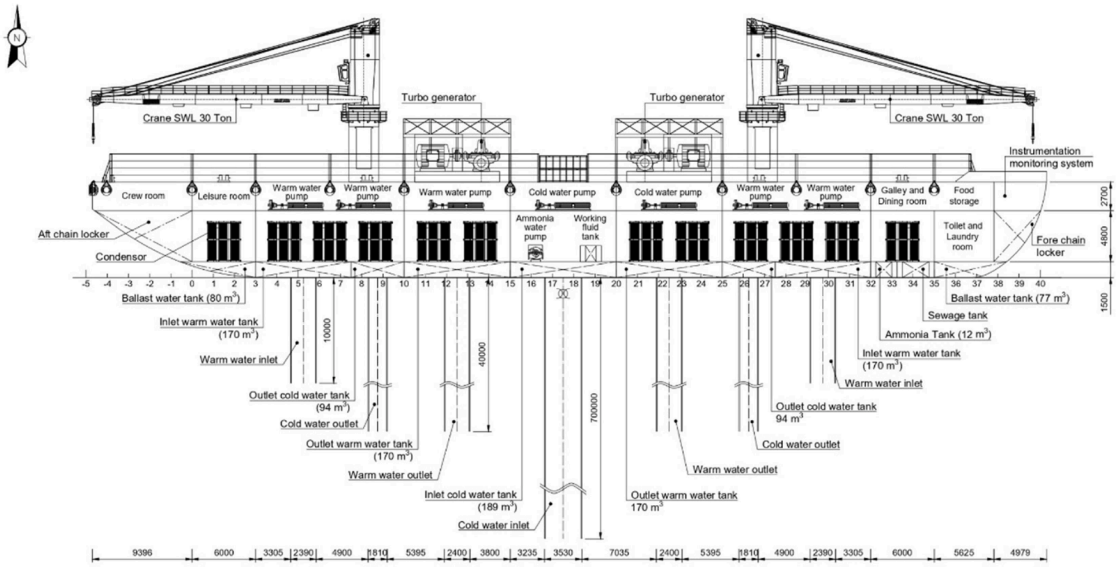

Fig. 9. Side View Prototype Floating Barge OTEC.

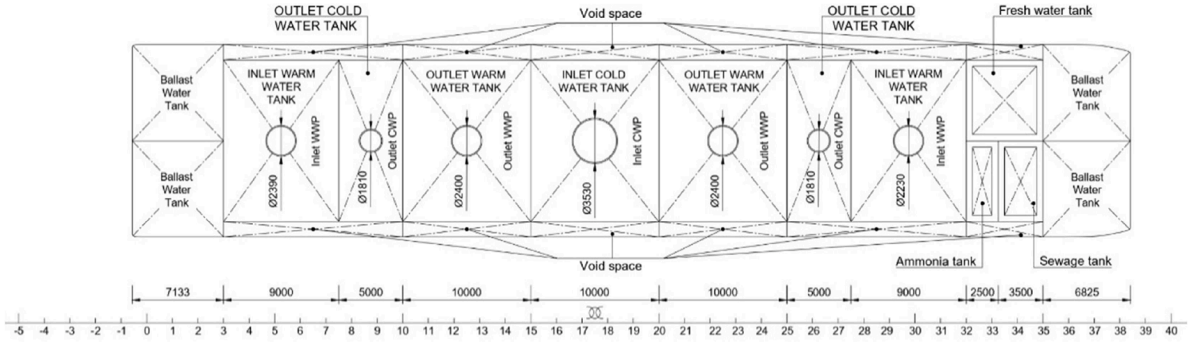

Fig. 10. Plan View Prototype Floating Barge OTEC 1500 mm.

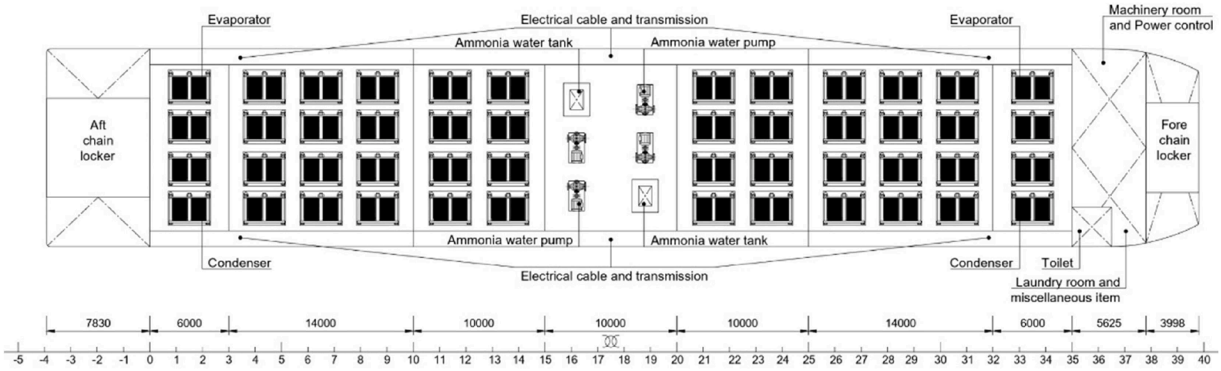

Fig. 11. Plan View Prototype Floating Barge OTEC 5300 mm.

system represents the largest cost share, reflecting the critical role of heat transfer efficiency in low-temperature OTEC cycles. Offshore infrastructure elements, including the floating barge, mooring system, and cold water pipe, also contribute significantly to the investment cost due to marine engineering requirements, structural stability considerations, and corrosion protection in seawater environments. These cost distributions are consistent with previous economic assessments of medium-scale floating OTEC systems reported in the literature [20]. Annual OPEX is estimated at 3% of CAPEX, or about Rp 59 billion per year, with a projected annual escalation of 2% due to energy inflation. The OPEX estimate includes routine maintenance of mechanical and electrical components, seawater pump operation, inspection of the cold water pipe and mooring system, as well as periodic cleaning of the heat exchangers using a Clean-in-Place (CIP) system to mitigate biofouling and scaling. The CIP process typically involves chemical cleaning cycles conducted every 3–6 months, depending on biofouling conditions in tropical seawater. These maintenance activities are incorporated within the 3% OPEX assumption commonly used in techno-economic analyses

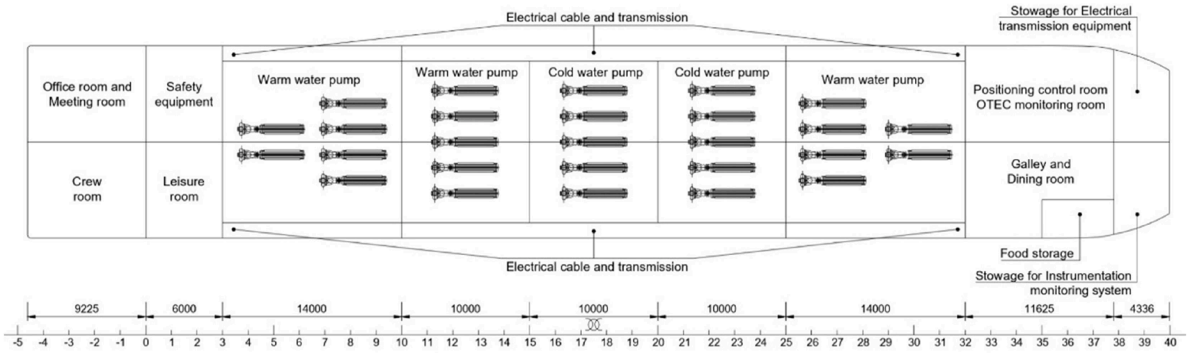

Fig. 12. Plan View Prototype Floating Barge OTEC 6300 mm.

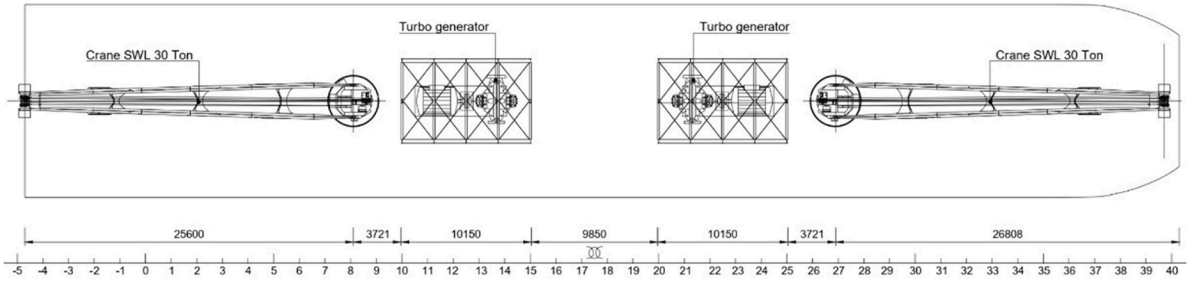

Fig. 13. Plan View Prototype Floating Barge OTEC 9000 mm.

of marine renewable energy systems. The relatively high CAPEX reflects the early-stage commercialization of OTEC technology and the marine engineering requirements of offshore deployment.

The levelized cost of energy (LCOE) is calculated using a discounted cash flow approach, which accounts for the time value of money over the project lifetime, following standard formulations widely applied in renewable energy economic assessments [21,22]. The LCOE is defined as:

$$LCOE_{Disconto} = \frac{CAPEX_t + \sum_{t=0}^{n} \frac{+OPEX_{total}}{(1+r)^t} - S_t}{\sum_{t=1}^{n} \frac{E_t}{(1+r)^t}}$$

where $CAPEX_t$ represents the investment cost, $OPEX_{total}$the operation and maintenance cost, S_t the salvage value, E_t the electricity generated in year t, r the discount rate, and $N$the project lifetime. For practical evaluation, a simplified formulation based on the capital recovery factor (CRF) is also applied, consistent with the methodology recommended by Langer [20], and is expressed as:

$$LCOE_{CRF} = \frac{CRF \times CAPEX + OPEX}{E_t}$$

with the CRF defined as:

$$\mathrm{CRF} = \frac{r(1+r)^N}{(1+r)^N - 1}$$

Using the CRF-based approach, the calculated LCOE is approximately Rp 2164/kWh, while the full discounted cash flow method yields an LCOE of Rp 2313/kWh. These values are competitive for marine renewable energy technologies and remain within the range of electricity generation costs in remote and island regions of Indonesia.

Project financing is assumed to follow a 70% debt and 30% equity structure, with a concessional loan interest rate of 3.5% and an 11-year repayment period. Under this scheme, the annual debt service is approximately Rp 159 billion. Based on electricity sales and operating costs, the equity payback period is estimated at approximately 4 years, while the total investment payback, including debt repayment, is achieved within 9 years.

In addition to electricity sales, the OTEC system offers co-benefits, including freshwater production, mariculture support, cold seawater-based cooling, and energy-related eco-tourism. These ancillary benefits contribute an estimated Rp 6 billion per year, further improving the overall economic attractiveness of the project and strengthening its socio-economic impact on coastal communities.

To evaluate the robustness of the economic results, a sensitivity analysis was conducted by varying several key parameters, including the discount rate, capital expenditure (CAPEX), and the temperature difference between warm and cold seawater. The analysis shows that CAPEX and discount rate are the most influential parameters affecting the levelized cost of energy (LCOE), while variations in the seawater temperature difference primarily affect the net power output and annual electricity generation. These findings highlight the importance of technological cost reductions and favorable financing mechanisms in improving the economic competitiveness of OTEC systems.

Overall, the economic assessment indicates that the proposed 11 MW OTEC system is financially viable, particularly in island regions with high electricity generation costs and growing demand for low-carbon baseload power. However, the commercialization of OTEC technology still faces several challenges, including high initial capital investment, limited industrial supply chains, and financing risks associated with emerging marine energy technologies. Continued technological development and supportive policy frameworks will therefore be essential for large-scale deployment.

6. Conclusions

This study presents a comprehensive technical and economic assessment of a floating closed-cycle OTEC system designed for deployment in North Bali waters. The analysis integrates thermodynamic cycle selection, offshore structural design, and long-term economic performance. The results show that the Uehara cycle achieves the highest thermal efficiency of 3.3% and the largest net power output of 11.724 MW, followed by the Rankine cycle with 11.086 MW and the

Kalina cycle with 10.081 MW. However, considering system simplicity, operational stability, and suitability for offshore implementation, the single Rankine cycle is selected as the basis for the floating OTEC prototype design in this study.

The proposed floating barge, mooring system, and cold-water pipe are shown to provide adequate stability and operational reliability under moderate sea conditions typical of North Bali. Heat exchangers are identified as the most critical components, significantly influencing both system efficiency and capital cost. From an economic perspective, the project exhibits competitive LCOE values, a reasonable payback period, and strong revenue stability due to continuous operation. The inclusion of OTEC co-benefits further enhances project viability and supports local economic development.

In conclusion, the proposed 11 MW floating OTEC system is technically feasible and economically promising, particularly for Indonesia's archipelagic regions where clean, reliable baseload power is urgently needed. With appropriate policy support, long-term power purchase agreements, and continued technological optimization, OTEC can become a strategic component of Indonesia's sustainable energy transition.

Future work will focus on a more detailed engineering analysis of the proposed floating OTEC system. This includes hydraulic analysis of the heat exchanger modules such as pressure drop, flow velocity, and flow distribution in parallel configurations. In addition, fouling effects on the seawater side and appropriate cleaning and maintenance strategies will be investigated.

Acknowledgement data availability

The authors confirm that the data supporting the findings of this study are available within the article.

CRediT authorship contribution statement

Ahmad M. Firdaus: Writing – review & editing, Validation, Supervision, Formal analysis, Conceptualization. **Adriani Phady:** Writing – original draft, Visualization, Investigation, Formal analysis, Data curation, Conceptualization. **Ristiyanto Adiputra:** Writing – review & editing, Validation, Supervision, Conceptualization.

Declaration of competing interest

The authors declare that they have no known competing financial interests or personal relationships that could have appeared to influence the work reported in this paper.

Acknowledgement

The authors would like to thank their appreciation to Lembaga Pengelola Dana Pendidikan (LPDP) for aiding us in the publication process and for publishing this paper.

This research was funded by the research and community service programme of Institut Technology Bandung (Program Penelitian dan Pengabdian Masyarakat -P2MI FTSL ITB) 2024

Data availability

Data will be made available on request.

References

[1] A.M. Firdaus, Tidal energy in Indonesia: opportunities and challenges, in: Ocean Renewable Energy, 8, American Society of Mechanical Engineers, Melbourne, Australia, 2023, https://doi.org/10.1115/OMAE2023-108028. V008T09A011.
[2] United Nations, Indonesia Population, Indonesia Population, 2025. Accessed: [Online]. Available: https://www.worldometers.info/world-population/indonesia-population/.
[3] R. Adiputra, T. Utsunomiya, J. Koto, T. Yasunaga, Y. Ikegami, Preliminary design of a 100 MW-net ocean thermal energy conversion (OTEC) power plant study case: mentawai island, Indonesia, J. Mar. Sci. Technol. 25 (1) (2020) 48–68, https://doi.org/10.1007/s00773-019-00630-7.
[4] S. Chang, R. Lei, J. He, X. Li, Y. Li, H. Hu, Numerical modelling and performance analysis of closed ocean thermal energy conversion cycles in the South China sea, Energy 316 (2025) 134591, https://doi.org/10.1016/j.energy.2025.134591.
[5] Yolanda, Studi Tekno Ekonomi Ocean Thermal Energy Conversion Di Selat Ombai, Nusa Tenggara Timur, Institut Teknologi Bandung, 2022.
[6] S.K. Gupta, A review on water–gas shift reactions energy production by carbon dioxide capture. *Sustainable Utilization of Carbon Dioxide:* From Waste to Product, 2023, pp. 195–205, d oi.org.
[7] B. Pemerintah Provinsi, Peraturan Daerah (Perda) Provinsi Bali Nomor 9 Tahun 2020 tentang Rencana Umum Energi Daerah Provinsi Bali Tahun 2020-2050," Bali, Peraturan Daerah Lampiran I, Peraturan Daerah Provinsi Bali Nomor 9 Tahun [Online]. Available, https://peraturan.bpk.go.id/Details/148301/perda-prov-bali-no-9-tahun-2020, 2020.
[8] D. Ilahude, A. Yuningsih, Y. Permanawati, M. Yosi, R. Zuraida, N. Annisa, Site determination for OTEC turbine installation of 100 MW capacity in North Bali Waters, Bull. Mar. Geol. 35 (1) (2020), https://doi.org/10.32693/bomg.35.1.2020.594.
[9] E.C. Yudananta, Perancangan Pembangkit Listrik Ocean Thermal Energy Conversion (OTEC) Di Daerah Bali Utara Sebagai Kawasan Energi Mandiri, Institut Teknologi Sepuluh Nopember, 2018.
[10] B. Pattanaik, S. Sutha, D. Dinesh, P. Jalihal, Data-driven model based adaptive feedback-feed forward control schemes for open cycle - OTEC process, Renew. Energy 221 (2024) 119765, https://doi.org/10.1016/j.renene.2023.119765.
[11] W. Gao, F. Wang, Y. Zhang, Z. Tian, D. Wu, S. Farrukh, Review of performance improvement strategies and technical challenges for ocean thermal energy conversion, Appl. Therm. Eng. 266 (2025) 125506, https://doi.org/10.1016/j.applthermaleng.2025.125506.
[12] Z. Hu, Y. Chen, Advancements in sustainable desalination with ocean thermal energy: a review, Desalination 586 (2024) 117770, https://doi.org/10.1016/j.desal.2024.117770.
[13] J. Herrera, S. Sierra, A. Ibeas, Ocean thermal energy conversion and other uses of deep sea water: a review, J. Mar. Sci. Eng. 9 (4) (2021) 356, https://doi.org/10.3390/jmse9040356.
[14] Y. Ikegami, T. Yasunaga, T. Morisaki, Ocean thermal energy conversion using double-stage rankine cycle, J. Mar. Sci. Eng. 6 (1) (2018) 21, https://doi.org/10.3390/jmse6010021.
[15] K.J. Rawson, E.C. Tupper (Eds.), Basic Ship Theory, 5th ed., Butterworth-Heinemann, Boston, 2001 [combined volume].
[16] ABS, Rules For Building and Classing Steel Barges, Rules for Building and Classing Steel Barges, USA, 2024.
[17] D.G.M. Watson, Practical Ship Design, Elsevier, 1998.
[18] BKI, Guidelines On Intact Stability, Jakarta, 2014.
[19] J. Langer, J. Quist, K. Blok, Upscaling scenarios for ocean thermal energy conversion with technological learning in Indonesia and their global relevance, Renew. Sustain. Energy Rev. 158 (2022) 112086, https://doi.org/10.1016/j.rser.2022.112086.
[20] J. Langer, A.A. Cahyaningwidi, C. Chalkiadakis, J. Quist, O. Hoes, K. Blok, Plant siting and economic potential of ocean thermal energy conversion in Indonesia a novel GIS-based methodology, Energy 224 (2021) 120121, https://doi.org/10.1016/j.energy.2021.120121.
[21] W. Short, D.J. Packey, and T. Holt, "A manual for the economic evaluation of energy efficiency and renewable energy technologies," NREL/TP–462-5173, 35391, 1995. doi: 10.2172/35391.
[22] IEA, IRENA, UNSD, The World Bank, and WHO, "Tracking SDG 7: The Energy Progress Report 2024," Washington, D.C., Jun. 2024. Accessed: Feb. 26, 2025. [Online]. Available: https://www.irena.org/Publications/2024/Jun/Tracking-SDG-7-The-Energy-Progress-Report-2024.